

Robust Wasserstein barycenter

Zixiong Cheng¹, Hang Liu^{1,✉}

¹ School of Management, University of Science and Technology of China, Jinzhai Rd, Hefei, 230026, Anhui Province

✉Corresponding Author(s): Hang Liu, hliu01@ustc.edu.cn

Graphical abstract

GraphicalAbstract content

Abstract

In this paper, we address a fundamental limitation of the classical Wasserstein barycenter—its sensitivity to outliers and its reliance on finite first/second moment assumptions. To overcome these issues, we propose the robust Wasserstein barycenter (RWB) based on a recent concept of the robust optimal transport. Theoretical guarantees, including existence and consistency, are established for the proposed RWB. Through extensive numerical experiments on both simulated and real-world data—including image processing and financial time series analysis—we demonstrate that the RWB exhibits superior robustness compared to the classical Wasserstein barycenter.

Keywords

Robust statistics; Wasserstein barycenter; optimal transport; outliers

1 Introduction

The theory of optimal transport (OT), first introduced by Monge [1] in the late 18th century, was revisited and generalized by Kantorovich [2] nearly two centuries later. Since the advent of efficient computational methods, OT has gained broad application across various disciplines, including machine learning and statistics. In machine learning, Arjovsky et al. [6] introduce WGAN as a GAN alternative, using Wasserstein distance to enhance training stability, which avoids mode collapse, and reveals deep connections to other distribution distances. In statistics, the Wasserstein

distance is utilized to quantify the discrepancy between probability distributions. Particularly in Compressive Statistical Learning (CSL), Vayer and Gribonval [19] provide a theoretical guarantee for the framework of compressive statistical learning by linking the Wasserstein distance to the Maximum Mean Discrepancy (MMD). Srivastava et al. [7] apply the Wasserstein distance in divide-and-conquer Bayesian inference, using barycenters of subset posterior distributions in Wasserstein space to efficiently approximate full-data posteriors with theoretical accuracy guarantees. Ramdas et al. [8] take the Wasserstein distance as the core in nonparametric two-sample testing to connect diverse univariate and multivariate testing methods via smoothed or distribution-free variants.

The Wasserstein barycenter is defined as the distribution that minimizes the sum of Wasserstein distances to a given set of distributions, and it offers an approach to averaging multiple distributions, generalizing the concept of central tendency to the space of probability measures.

Le Gouic [11] establishes the existence and consistency of the p -Wasserstein barycenter, thereby providing a rigorous theoretical foundation for its application. Meanwhile, Cuturi and Doucet [15] demonstrate the computational efficiency and practical utility of the Wasserstein barycenter, yielding remarkable applications such as image recognition and clustering. Despite its wide applications in statistics, economics, and machine learning, the Wasserstein barycenter exhibits some fundamental issues: it requires finite first or second moments of the distributions; it is sensitive to outliers and contaminations. In conventional dataset-related problems, robustness is typically achieved by removing extreme values; however, the Wasserstein barycenter, which is defined as the center of mass with respect to a collection of probability measures, complicates the identification of outliers.

In Ma et al. [4], the robust Wasserstein distance is defined by introducing the concept of robust optimal transport (ROT) in Mukherjee et al. [13], which truncates the distance function integrated in the computation of the Wasserstein distance, thus ensuring the robustness of the distance measure. Notably, this framework considers only the robust version of the classical W_p distance for $p = 1$. We generalize the

robust Wasserstein distance to the case of $p \geq 1$ and introduce the robust Wasserstein barycenter (RWB) as a robust alternative to classical Wasserstein barycenter (WB). Unlike the WB, our RWB does not impose any moment assumption on the probability measures. Extensive experiments demonstrate enhanced robustness of the RWB compared to the WB. For the computation of the WB, Lindheim [20] notes that although the IBP algorithm [10] is highly efficient and straightforward in most cases, it is a fixed-support method implemented on a grid, thus has the issue of the curse of dimensionality. In contrast, barycenters without such constraints are referred to as free-support barycenters. Since the optimal solution is inherently sparse, free-support approach can overcome the curse of dimensionality. Our findings reveal that the free-support method, beyond its previously acknowledged advantage of overcoming the curse of dimensionality, also optimizes the barycenter results in processing images. Therefore, we utilize the simple and well known fixed-point algorithm mentioned in Lindheim [20] to enhance the results of the fixed-support IBP algorithm in our experiments.

The structure of the paper is organized as follows. Section 2 collects essential concepts related to the robust Wasserstein barycenter, including optimal transport, the Fréchet mean, the robust Wasserstein distance and so on. Section 3 proposes the new concept of the RWB and proves the existence and consistency of the RWB. Section 4 introduces a free-support algorithm for computing the RWB, which is built on existing fixed-support algorithms. Finally, Section 5 compares the RWB and WB through simulation and real-data analysis, illustrating the advantages of the RWB.

The main contributions of this paper are three-folds:

- (i) We propose the novel concept of the robust Wasserstein barycenter that overcomes the robustness issue of the classical Wasserstein barycenter.
- (ii) We prove the existence and consistency of the RWB. Furthermore, we characterize the size of the support of the robust Wasserstein barycenter under the condition that all input distributions are discrete with finite supports.
- (iii) We propose a free-support algorithm that generalizes fixed-support algorithms, thereby addressing the challenge that fixed-support algorithms face in determin-

ing an appropriate support for the barycenter in high-dimensional scenarios.

2 Preliminaries

In this section, we introduce concepts of the Fréchet mean, optimal transport and Wasserstein distance that are relevant for the definition of robust Wasserstein barycenter.

2.1 Fréchet mean

Given a metric space (\mathcal{X}, d) and a positive integer k , k -Fréchet mean introduced in [3] is defined for a random variable $X \in \mathcal{X}$ as

$$\theta_k := \arg \min_{x \in \mathcal{X}} \mathbb{E}[d^k(X, x)].$$

The k -Fréchet mean generalizes the concept of the mean from Euclidean space to generic metric spaces. When (\mathcal{X}, d) is Euclidean, the k -Fréchet mean coincides with some well-known measures of central tendency: for $k = 1$, it corresponds to the usual median, and for $k = 2$, it corresponds to the arithmetic mean.

Given observations X_1, \dots, X_n that are i.i.d. copies of X , the *empirical k -Fréchet mean* is naturally defined as

$$\hat{\theta}_k := \arg \min_{x \in \mathcal{X}} \sum_{i=1}^n d^k(X_i, x).$$

2.2 Optimal transport

Let (\mathcal{X}, d) and (\mathcal{Y}, d) be two complete and separable metric spaces, and let $\mathcal{P}(\mathcal{X})$ denote the set of all probability measures on \mathcal{X} . Given two probability measures $\mu \in \mathcal{P}(\mathcal{X})$, $\nu \in \mathcal{P}(\mathcal{Y})$ and a cost function $c : \mathcal{X} \times \mathcal{Y} \rightarrow [0, +\infty]$, the optimal transport problem first proposed by [1] is to solve the following minimization equation

$$\inf \left\{ \int_{\mathcal{X}} c(x, \mathcal{T}(x)) d\mu(x) : \mathcal{T} \# \mu = \nu \right\},$$

where $\mathcal{T} \# \mu = \nu$ indicates that \mathcal{T} pushes μ forward to ν . While Monge's concept of finding a push-forward map that minimizes the total transport cost is quite intuitive, it faces two critical limitations that hinder its practical implementation. First,

solutions may not exist for certain measures. For example, no map can push a discrete probability measure forward to a continuous one. Second, the set $\{\mu, \mathcal{T}(\nu)\}$ of all measurable transport map is non-convex, which makes Monge's minimization problem computationally challenging.

Monge's problem is revisited by Kantorovich [2], which proposes a more flexible and computationally feasible formulation. Let $\Pi(\mu, \nu)$ denote the set of all joint probability measures of $\mu \in \mathcal{P}(\mathcal{X})$ and $\nu \in \mathcal{P}(\mathcal{Y})$. Kantorovich's problem aims to find a joint distribution $\gamma \in \Pi(\mu, \nu)$ that provides the optimal coupling between X and Y , which is formulated as

$$\inf \left\{ \int_{\mathcal{X} \times \mathcal{Y}} c(x, y) d\gamma(x, y) : \gamma \in \Pi(\mu, \nu) \right\}.$$

Let $\mathcal{P}_p(\mathcal{X}) = \{\mu \in \mathcal{P}(\mathcal{X}) : \int_{\mathcal{X}} d^p(x, x_0) d\mu < +\infty \text{ for some } x_0 \in \mathcal{X}\}$ denote the set of all probability measures on \mathcal{X} with finite moment of order p ($p \in [1, +\infty)$). Given two probability measures $\mu, \nu \in \mathcal{P}_p(\mathcal{X})$, the p -Wasserstein distance $W_p(\mu, \nu)$ is defined as the minimal value of the optimal transport problem, that is,

$$W_p(\mu, \nu) := \inf_{\gamma \in \Pi(\mu, \nu)} \left\{ \int_{\mathcal{X} \times \mathcal{X}} d^p(x, y) d\gamma \right\}^{\frac{1}{p}}.$$

In contrast to the Kullback-Leibler (KL) divergence [17] and the Jensen-Shannon (JS) divergence [18], the Wasserstein distance is a metric between probability measures. Consequently, \mathcal{P}_p , when endowed with W_p , is a metric space referred to as the Wasserstein space [23]. Another advantage of the Wasserstein distance over the KL divergence is that the latter is well-defined only if two probability measures have the same support, whereas the former can be applied to probability measures with different supports.

3 Robust Wasserstein barycenter

In this section, building upon the robust optimal transport in [13] and [4], we introduce the robust Wasserstein distance $W_p^{(\lambda)}$ as a robust version of the classical Wasserstein distance W_p . Based on $W_p^{(\lambda)}$, we propose the concept of the robust Wasserstein barycenter (RWB) and establish the existence and consistency of the RWB.

3.1 Robust Wasserstein distance

Since the Wasserstein distance requires finite p -th-order moments and is sensitive to outliers, the main idea of the robust optimal transport frameworks in [13] and [4] is to truncate the cost function of the classical W_1 distance, thereby yielding the minimization problem

$$\inf_{\gamma \in \Pi(\mu, \nu)} \left\{ \int_{\mathcal{X} \times \mathcal{X}} c^{(\lambda)}(x, y) d\gamma \right\},$$

where

$$c^{(\lambda)}(x, y) := \min\{d(x, y), \lambda\}, \quad (1)$$

with $\lambda > 0$ as a regularization parameter controlling the truncation level. According to [4], since $c^{(\lambda)}$ is a metric on \mathcal{X} , the robust Wasserstein distance is defined as

$$W^{(\lambda)}(\mu, \nu) := \min_{\gamma \in \Pi(\mu, \nu)} \left\{ \int_{\mathcal{X} \times \mathcal{X}} c^{(\lambda)}(x, y) d\gamma \right\},$$

which is a metric on $\mathcal{P}(\mathcal{X})$ and coincides with the classical W_1 distance on the space of probability measures over the metric space $(\mathcal{X}, c^{(\lambda)})$.

We consider a p -th generalized version of $W^{(\lambda)}$ and define the *robust W_p distance* ($p \geq 1$) as

$$W_p^{(\lambda)}(\mu, \nu) := \min_{\gamma \in \Pi(\mu, \nu)} \left\{ \int_{\mathcal{X} \times \mathcal{X}} [c^{(\lambda)}(x, y)]^p d\gamma \right\}^{\frac{1}{p}}.$$

Similar to $W^{(\lambda)}$, $W_p^{(\lambda)}$ is a metric on $\mathcal{P}(\mathcal{X})$, and it does not require any moment assumption on the probability measure. We refer to $\mathcal{P}(\mathcal{X})$ endowed with the metric $W_p^{(\lambda)}$ as the *p -th robust Wasserstein space*, which we denote as $\mathcal{W}_p^{(\lambda)}(\mathcal{X})$. The most commonly adopted values for p are $p = 1$ and $p = 2$. As noted in [23], the W_1 Wasserstein distance is more robust and less sensitive to outliers, whereas the W_2 Wasserstein distance exhibits superior geometric properties and is more computationally efficient. In our experiments, we find that the robust Wasserstein distance also exhibits the previously mentioned characteristics, and we conjecture that this may be attributed to differences in the cost matrix.

3.2 Robust Wasserstein barycenter

Now we propose the robust Wasserstein barycenter, which, unlike the classical Wasserstein barycenter, does not impose any finite moment assumptions on the probability measures.

Definition 1. Let Λ denote a random probability measure on $\mathcal{W}_p^{(\lambda)}(\mathcal{X})$. The robust Wasserstein barycenter $\nu_{p,k}^{(\lambda)}$ ($k \geq 1$) of Λ can be defined as

$$\nu_{p,k}^{(\lambda)} := \arg \min_{\xi \in \mathcal{W}_p^{(\lambda)}(\mathcal{X})} \mathbb{E} \left[W_p^{(\lambda)}(\Lambda, \xi) \right]^k.$$

Let $\mu_i \in \mathcal{W}_p^{(\lambda)}(\mathcal{X})$, $i = 1, \dots, n$, be a sequence of probability measures. The RWB with respect to $\Lambda = \sum_{i=1}^n w_i \delta_{\mu_i}$ can be written as :

$$\nu_{p,k}^{(\lambda,n)} := \arg \min_{\xi \in \mathcal{W}_p^{(\lambda)}(\mathcal{X})} \mathbb{E} \left[W_p^{(\lambda)} \left(\sum_{i=1}^n w_i \delta_{\mu_i}, \xi \right) \right]^k = \arg \min_{\xi \in \mathcal{W}_p^{(\lambda)}(\mathcal{X})} \sum_{i=1}^n w_i \left[W_p^{(\lambda)}(\delta_{\mu_i}, \xi) \right]^k,$$

where $\{\delta_{\mu_i}\}_{i=1}^n$ denotes a sequence of Dirac measures, each concentrated at a point μ_i in $\mathcal{W}_p^{(\lambda)}(\mathcal{X})$. The weights w_i for $i = 1, \dots, n$, satisfy $\sum_{i=1}^n w_i = 1$, ensuring that $\sum_{i=1}^n w_i \delta_{\mu_i}$ is a valid random measure. Additionally, in applications, it is typical to set $k = p$, which is the most common form of the Wasserstein barycenter and satisfies the requirements for most scenarios.

The following result establishes the existence of the RWB of any $\Lambda \in \mathcal{W}_p^{(\lambda)}(\mathcal{X})$.

Proposition 1 (Existence). For any $k \geq 1$, the functional $F(\nu) = \mathbb{E} \left[W_p^{(\lambda)}(\nu, \Lambda) \right]^k$ associated with any random probability measure Λ on $\mathcal{W}_p^{(\lambda)}(\mathcal{X})$ admits a minimizer ν^* .

Proof. Obviously, for any $\nu \in \mathcal{W}_p^{(\lambda)}(\mathcal{X})$, the functional

$$F(\nu) = \mathbb{E} \left[W_p^{(\lambda)}(\nu, \Lambda) \right]^k \leq \lambda < \infty.$$

We can take a minimizing sequence $\{\nu_j\} \subset \mathcal{W}_p^{(\lambda)}(\mathcal{X})$. For any $R > 0$ and any fixed point $x_0 \in \mathcal{X}$, by the Chebyshev's inequality we have that

$$\nu_j \left(\left\{ x \in \mathcal{X} \mid c^{(\lambda)}(x, x_0) \geq R \right\} \right) \leq \frac{1}{R} \int_{\{x: c^{(\lambda)}(x, x_0) \geq R\}} c^{(\lambda)}(x, x_0) d\nu_j(x) \leq \frac{\lambda}{R}.$$

For any $\epsilon > 0$, we can choose a sufficiently large R such that $R > \lambda/\epsilon$. In fact, we might let $\epsilon < 1$, then $R > \lambda$. For the closed ball

$$B_R(x_0) = \left\{ x \in \mathcal{X} \mid c^{(\lambda)}(x, x_0) \leq R \right\} = \mathcal{X},$$

we have $\nu_j(B_R) = 1 > 1 - \epsilon$, for any j .

The sequence of measures $\{\nu_j\}$ is tight since $(\mathcal{X}, c^{(\lambda)})$ is a complete, separable and compact metric space. By the Prokhorov's theorem [24], there exists a subsequence $\{\nu_{j_i}\}$ that converges weakly to some $\nu^* \in \mathcal{W}_p^{(\lambda)}(\mathcal{X})$. Then we have

$$\begin{aligned} F(\nu^*) &= \mathbb{E} \left[W_p^{(\lambda)}(\nu^*, \Lambda) \right]^k \\ &\leq \mathbb{E} \liminf_{j_i \rightarrow \infty} \left[W_p^{(\lambda)}(\nu_{j_i}, \Lambda) \right]^k \\ &\leq \liminf_{j_i \rightarrow \infty} \mathbb{E} \left[W_p^{(\lambda)}(\nu_{j_i}, \Lambda) \right]^k \\ &= \inf F, \end{aligned}$$

where the first inequality is due to the lower semicontinuity of the Wasserstein distance [16, Equation 2.5], and the second inequality is a consequence of Fatou's lemma. This completes the proof. \square

Moreover, we also establish the consistency of the RWB, which is stated as follows.

Proposition 2 (Consistency). Let Λ_j on $W_p^{(\lambda)}(\mathcal{X})$, $j \in \mathbb{N}$ be a sequence of random measures with a sequence of robust Wasserstein barycenters $\nu_{p,k,j}^{(\lambda)}$ ($k, p \geq 1$). Assuming that $W_p^{(\lambda)}(\Lambda_j, \Lambda) \rightarrow 0$ for a random measure Λ on $W_p^{(\lambda)}(\mathcal{X})$ as $j \rightarrow \infty$. Then the sequence $\{\nu_{p,k,j}^{(\lambda)}\}$ is tight and any limit is a robust Wasserstein barycenter of Λ .

Proof. According to the proof of Proposition 1, the sequence of robust Wasserstein barycenters $\{\nu_{p,k,j}^{(\lambda)}\}$ is tight. We can take any subsequence $\{\nu_{p,k,j_i}^{(\lambda)}\}$ that weakly converges to some $\nu^* \in \mathcal{W}_p^{(\lambda)}(\mathcal{X})$.

Next, we will prove that the point ν^* is also a robust Wasserstein barycenter. Consider random measures μ_{j_i} and μ , which are random copies of Λ_{j_i} and Λ , respectively. Then we aim to prove that $\mathbb{E} \left[W_p^{(\lambda)}(\xi, \mu) \right]^k \geq \mathbb{E} \left[W_p^{(\lambda)}(\nu^*, \mu) \right]^k$ holds for

any choice of $\xi \in \mathcal{W}_p^{(\lambda)}(\mathcal{X})$.

$$\begin{aligned}
\mathbb{E} \left[W_p^{(\lambda)}(\xi, \mu) \right]^k &= \left[W_p^{(\lambda)}(\delta_\xi, \Lambda) \right]^k \\
&= \lim_{j_l \rightarrow \infty} \left[W_p^{(\lambda)}(\delta_\xi, \Lambda_{j_l}) \right]^k \\
&= \lim_{j_l \rightarrow \infty} \mathbb{E} \left[W_p^{(\lambda)}(\xi, \mu_{j_l}) \right]^k \\
&\geq \lim_{j_l \rightarrow \infty} \mathbb{E} \left[W_p^{(\lambda)}(\nu_{p,k,j_l}^{(\lambda)}, \mu_{j_l}) \right]^k \\
&\geq \mathbb{E} \liminf_{j_l \rightarrow \infty} \left[W_p^{(\lambda)}(\nu_{p,k,j_l}^{(\lambda)}, \mu_{j_l}) \right]^k \text{ by Fatou's lemma} \\
&\geq \mathbb{E} \left[W_p^{(\lambda)}(\nu^*, \mu) \right]^k.
\end{aligned} \tag{2}$$

The first inequality holds because every element in the sequence $\{\nu_{p,k,j_l}^{(\lambda)}\}$ is a robust Wasserstein barycenter that minimizes the expected robust Wasserstein distance to the random measure $\{\Lambda_{j_l}\}$. The last inequality holds because the Wasserstein distance is lower semicontinuous and the robust Wasserstein distance is a special case of the Wasserstein distance. Furthermore, the convergence of $\Lambda_{j_l} \rightarrow \Lambda$ allows us to construct $\mu_{j_l} \rightarrow \mu$ almost surely by Skorokhod's representation theorem in [5].

We then aim to further prove $W_p^{(\lambda)}(\nu_{p,k,j_l}^{(\lambda)}, \nu^*) \rightarrow 0$. If $\xi = \nu^*$, Equation (2) is in fact an equality, which implies that $W_p^{(\lambda)}(\delta_{\nu_{p,k,j_l}^{(\lambda)}}, \Lambda_{j_l}) \rightarrow W_p^{(\lambda)}(\delta_{\nu^*}, \Lambda)$. By the triangle inequality, we have

$$\begin{aligned}
&W_p^{(\lambda)}(\delta_{\nu_{p,k,j_l}^{(\lambda)}}, \Lambda) - W_p^{(\lambda)}(\delta_{\nu^*}, \Lambda) \\
&\leq W_p^{(\lambda)}(\delta_{\nu_{p,k,j_l}^{(\lambda)}}, \Lambda_{j_l}) + W_p^{(\lambda)}(\Lambda_{j_l}, \Lambda) - W_p^{(\lambda)}(\delta_{\nu^*}, \Lambda) \rightarrow 0.
\end{aligned}$$

Since ν^* is a minimizer of $\mathbb{E}W_p^{(\lambda)}(\nu, \Lambda)$, we have $\left[W_p^{(\lambda)}(\delta_{\nu_{p,k,j_l}^{(\lambda)}}, \Lambda) \right]^k \geq \left[W_p^{(\lambda)}(\delta_{\nu^*}, \Lambda) \right]^k$,

which implies $W_p^{(\lambda)}(\delta_{\nu_{p,k,j_l}^{(\lambda)}}, \Lambda) - W_p^{(\lambda)}(\delta_{\nu^*}, \Lambda) \geq 0$. Moreover, we have

$$\liminf_{j_l \rightarrow \infty} W_p(\nu_{p,k,j_l}^{(\lambda)}, \mu) = W_p(\nu^*, \mu),$$

which implies $W_p^{(\lambda)}(\nu_{p,k,j_l}^{(\lambda)}, \xi) \rightarrow W_p^{(\lambda)}(\nu^*, \xi)$ for any $\xi \in \mathcal{P}_p(\mathcal{X})$ almost surely with respect to Λ . By the Theorem 2.2.1 in [16], it is equivalent to $W_p^{(\lambda)}(\nu_{p,k,j_l}^{(\lambda)}, \nu^*) \rightarrow 0$, which completes the proof.

Hence, any limit point of $\{\nu_{p,k,j}^{(\lambda)}\}$ is indeed a robust Wasserstein barycenter of Λ . \square

Remark 1. If Λ is approximated by a growing discrete distribution $\Lambda^{(j)} = \sum_{i=1}^j w_i^{(j)} \delta_{\mu_i^{(j)}}$, then the sequence of barycenters $\{\nu_{p,k,j}^{(\lambda)}\}$ is tight, and any limit point is a robust Wasserstein barycenter of Λ .

Remark 2. Chewi et al. [26] characterize the uniqueness of Wasserstein barycenters via geometric conditions and optimal transport theory [Sections 8.2–8.3], and further identifies the strict convexity of $\mathbb{E}[W_p(\nu, \Lambda)]^k$ as the core reason for the uniqueness of Wasserstein barycenters. However, due to the truncation parameter λ , the objective function $F(\nu) = \mathbb{E}[W_p^{(\lambda)}(\nu, \Lambda)]^k$ fails to be strictly convex. Consequently, the robust Wasserstein barycenter which is regarded as a specific subclass of the Wasserstein barycenter may not be unique in general cases.

4 Computation algorithms

The Wasserstein barycenter is an effective tool for summarizing collections of probability distributions and has wide applications in machine learning and statistics. However, computing the Wasserstein barycenter is quite challenging, as it involves solving a high-dimensional linear optimization problem. Altschuler and Boix-Adser [9] characterize the curse of dimensionality for the Wasserstein barycenter and proves that its computation is NP-hard.

The majority of algorithms constrain the support of the barycenter to a predetermined set of grid points to compute the optimal probability mass distribution and such methods are referred to as *fixed-support* algorithms. Notably, the Iterative Bregman Projections (IBP) algorithm proposed in [10] is one of the most widely used fixed-support algorithm. While the IBP algorithm exhibits remarkable efficiency and simplicity in low-dimensional cases, it suffers from the curse of dimensionality due to its reliance on a fixed grid. Specifically, the number of support points for such a grid increases exponentially as the dimension increases. Although the support size of the Wasserstein barycenter exhibits sparsity under the assumption that all input

distributions have finite support (see e.g. Carlier and Ekeland [21] and Friesecke and Penka [22]), it is difficult for fixed-support methods to find a suitable sparse support.

Fortunately, *free-support algorithms* optimize for both the probability mass weights and the support of the barycenter. This enables the number of support points to be much smaller than that of the full grid, thus effectively alleviating the curse of dimensionality in high-dimensional cases (see e.g. Cuturi and Doucet [15] and Lindheim [20]). Additionally, we find that the free-support variant of IBP performs better than the original IBP in image processing experiments.

To this end, we first note that the robust Wasserstein barycenter has a finite support when the input distributions admit finite supports, and then introduce free-support methods for computing the RWB.

4.1 Support of RWB

In the following, $\{\mu_i\}_{i=1}^n$ and ν denote some finite discrete probability measures in $\mathcal{W}_p^{(\lambda)}(\mathcal{X})$, and $\Delta_m := \{u \in \mathbb{R}^m \mid u_i \geq 0 \text{ for all } i, \sum_{i=1}^m u_i = 1\}$ denotes a set of values for probability mass weight. Then we assume that each μ_i is supported on $\text{supp}(\mu_i) = \{x_1^{(i)}, \dots, x_{S_i}^{(i)}\} \subset \mathcal{X}$, so we can denote each $\mu_i = \sum_{s=1}^{S_i} q_s^{(i)} \delta_{x_s^{(i)}}$, where $S_i = |\text{supp}(\mu_i)|$ denotes the support size of μ_i and $q^{(i)} = (q_1^{(i)}, \dots, q_{S_i}^{(i)}) \in \Delta_{S_i}$ denotes the probability mass weight of μ_i on $\text{supp}(\mu_i)$.

In practice it is common to set $k = p$ for the RWB $\nu_{p,k}^{(\lambda)}$, similar to the classical WB. We therefore focus on the $\nu_{p,p}^{(\lambda)}$. For convenience, let $\nu_p^{(\lambda)}$ denote $\nu_{p,p}^{(\lambda)}$, which is the solution to the optimization problem:

$$\begin{aligned} & \arg \min_{\nu \in \mathcal{W}_p^{(\lambda)}(\mathcal{X})} f(\nu), \\ & f(\nu) = \sum_{i=1}^n w_i \left[W_p^{(\lambda)}(\nu, \mu_i) \right]^p, \end{aligned} \quad (3)$$

where $\{w_i\}_{i=1}^n$ is a sequence of non-negative weights satisfying $\sum_{i=1}^n w_i = 1$.

The following theorem, which relies on Carlier and Ekeland [21, Prop. 3] and Friesecke and Penka [22, Thm. 1], establishes a theoretical connection between Wasserstein barycenter problems and multi-marginal optimal transport. It further

characterizes the support of WB and extends the corresponding theoretical framework to the RWB, as the RWB is a special case of the WB.

Theorem 1. According to Proposition 1, equation (3) admits at least one solution, which is the RWB $\nu_p^{(\lambda)}$, and we have that:

$$\text{supp} \left(\nu_p^{(\lambda)} \right) \subseteq \arg \min_{y \in \mathcal{X}} \left\{ \sum_{i=1}^n w_i c^{(\lambda)} \left(y, x^{(i)} \right) \mid \forall x^{(i)} \in \text{supp}(\mu_i), i = 1, \dots, n \right\} \quad (4)$$

Moreover, there exists an optimal solution $\nu_p^{(\lambda)*}$ s.t.

$$|\text{supp} \left(\nu_p^{(\lambda)*} \right)| \leq \sum_{i=1}^n S_i + 1 - n.$$

This theorem not only helps choose a suitable support for fixed-support algorithms in RWB computation, but also provides an upper bound on the support size for free-support algorithms.

4.2 Free-support methods

As noted above, we have that $\text{supp}(\mu_i) = \{x_1^{(i)}, \dots, x_{S_i}^{(i)}\} \subset \mathcal{X}$ and $\mu_i = \sum_{s=1}^{S_i} q_s^{(i)} \delta_{x_s^{(i)}}$, i.e., for $i = 1, \dots, n$. By Theorem 1, the support of $\nu_p^{(\lambda)}$ in (3) is finite, so we may write $\text{supp}(\nu_p^{(\lambda)}) = \{y_1, \dots, y_R\}$ and $\nu_p^{(\lambda)} = \sum_{r=1}^R p_r \delta_{y_r}$, where $y_r \in \mathcal{X}$ and $p = (p_1, \dots, p_R) \in \Delta_R$.

For $i = 1, \dots, n$, let Π^i denote the optimal transports plan $\Pi \left(\nu_p^{(\lambda)}, \mu_i \right)$, i.e.,

$$\Pi^i = \sum_{r=1}^R \sum_{s=1}^{S_i} \pi_{rs}^{(i)} \delta \left(y_r, x_s^{(i)} \right),$$

where $\pi_{rs}^{(i)}$ minimizes $\sum_{r=1}^R \sum_{s=1}^{S_i} \pi_{rs}^{[i]} c^{(\lambda)} \left(y_r, x_s^{(i)} \right)$ and $\pi_{rs}^{[i]}$ denotes the weight of the coupling $\Pi \left(\nu_p^{(\lambda)}, \mu_i \right)$ at $\left(y_r, x_s^{(i)} \right)$.

Given that $\pi^i = \left(\pi_{rs}^{(i)} \right)_{R \times S_i}$ and $\pi := \left(\pi^1, \dots, \pi^n \right) = \left(\pi_{rs}^{(i)} \right)_{n \times R \times S_i}$, and we define a map $B_{\nu_p^{(\lambda)}} : \text{supp} \left(\nu_p^{(\lambda)} \right) \rightarrow \mathcal{X}$ as follows:

$$b_r \triangleq B_{\nu_p^{(\lambda)}} \left(y_r \right) := \arg \min_{z \in \mathcal{X}} \sum_{i=1}^n w_i \sum_{s=1}^{S_i} \pi_{rs}^{(i)} c^{(\lambda)} \left(z, x_s^{(i)} \right), \quad r = 1, \dots, R. \quad (5)$$

In general, w_i ($i = 1, \dots, n$) is set to $\frac{1}{n}$ so we have

$$b_r = \arg \min_{z \in \mathcal{X}} \sum_{i=1}^n \sum_{s=1}^{S_i} \pi_{rs}^{(i)} c^{(\lambda)}(z, x_s^{(i)}), \quad r = 1, \dots, R.$$

Furthermore, we can define the new discrete measure as: $b(\nu_p^{(\lambda)}) := \sum_{r=1}^R p_r \delta_{b_r}$.

Remark 4.2 Note that $\sum_{i=1}^n \sum_{s=1}^{S_i} \pi_{rs}^{(i)} c^{(\lambda)}(z, x_s^{(i)})$ is convex, which ensures the existence of b_r for $r = 1, \dots, R$.

Theorem 2. For $\nu_p^{(\lambda)}$ and $b(\nu_p^{(\lambda)})$, we have:

$$f(b(\nu_p^{(\lambda)})) \leq f(\nu_p^{(\lambda)}),$$

where $f(\cdot)$ is defined in (3).

Proof. Let $\Pi = \sum_{i=1}^n \sum_{r=1}^R \sum_{s=1}^{S_i} \pi_{rs}^{(i)} \delta(b_r, x_s^{(i)})$ denote the transport plan between $\nu_p^{(\lambda)}$ and $\{\mu_i\}_{i=1}^n$, and $\hat{\Pi} = \sum_{i=1}^n \sum_{r=1}^R \sum_{s=1}^{S_i} \hat{\pi}_{rs}^{(i)} \delta(b_r, x_s^{(i)})$ denote the transport plan between $b(\nu_p^{(\lambda)})$ and $\{\mu_i\}_{i=1}^n$. Then we have that:

$$\begin{aligned} f(b(\nu_p^{(\lambda)})) &= \sum_{i=1}^n w_i W_p^{(\lambda)}(b(\nu_p^{(\lambda)}), \mu_i) \\ &= \sum_{i=1}^n w_i \sum_{r=1}^R \sum_{s=1}^{S_i} \hat{\pi}_{rs}^{(i)} c^{(\lambda)}(b_r, x_s^{(i)}) \\ &\leq \sum_{i=1}^n w_i \sum_{r=1}^R \sum_{s=1}^{S_i} \pi_{rs}^{(i)} c^{(\lambda)}(b_r, x_s^{(i)}) \\ &= \sum_{r=1}^R \sum_{i=1}^n w_i \sum_{s=1}^{S_i} \pi_{rs}^{(i)} c^{(\lambda)}(b_r, x_s^{(i)}) \\ &= \sum_{r=1}^R \arg \min_{z \in \mathcal{X}} \sum_{i=1}^n w_i \sum_{s=1}^{S_i} \pi_{rs}^{(i)} c^{(\lambda)}(z, x_s^{(i)}) \\ &\leq \sum_{r=1}^R \sum_{i=1}^n w_i \sum_{s=1}^{S_i} \pi_{rs}^{(i)} c^{(\lambda)}(y_r, x_s^{(i)}) \\ &= \sum_{i=1}^n w_i W_p^{(\lambda)}(\nu_p^{(\lambda)}, \mu_i) \\ &= f(\nu_p^{(\lambda)}) \end{aligned}$$

□

Remark 4.3 Given an arbitrary discrete probability measure ν , we set $\nu_0 = \nu_p^{(\lambda)}$, $\nu_k = b(\nu_{k-1})$, $k = 1, 2, \dots$, then we can have $f(\nu_p^{(\lambda)}) \geq f(\nu_1) \geq f(\nu_2) \geq \dots \geq 0$. Moreover, $\{f(\nu_k)\}$ converges by the monotone bounded convergence theorem.

Since the RWB is a special case of the WB, many fixed-support algorithms of WB—including Iterative Bregman Projections (IBP)[10]—can be adapted to the RWB. According to Theorem 2, replacing the measure $\nu_p^{(\lambda)}$ obtained by any fixed-support algorithm with $b(\nu_p^{(\lambda)})$ can reduce the sum of robust Wasserstein distances between the barycenter and input distributions. Additionally, it is clear that the conclusions in this section apply not only to the robust Wasserstein space but also to other Wasserstein spaces. Algorithm 1 provides the pseudocode of the free-support method.

Algorithm 1 Free-support method for RWB

Input: A sequence of discrete probability masses $\{\mu_i\}_{i=1}^n$ and their supports $\{\text{supp}(\mu_i)\}_{i=1}^n$, the cost function $c^{(\lambda)}(\cdot, \cdot)$, the original support of RWB supp_0

- 1: **while** not converge **do**
- 2: Compute the optimal mass ν_{mass} by fixed-support algorithm
- 3: Update the support supp_{new} by (5)
- 4: **end while**

Output: ν_{mass} is the mass of RWB $\nu_p^{(\lambda)}$, and supp_{new} is the support of $\nu_p^{(\lambda)}$

5 Numerical results

5.1 Comparison of image processing

As the method in Section 4 satisfies the aforementioned requirements and computational constraints, computational cost limitations, coupled with the focus of our work on comparing the performance differences between the WB and RWB, lead us to omit high-dimensional numerical experiments that demonstrate the free-support approach’s ability to overcome the curse of dimensionality. Experiments in this section are thus restricted to low-dimensional image processing scenarios. The high-dimensional performance of the proposed method can be theoretically inferred from its sparsity and

computational framework, and will be verified in future work with more sufficient computational resources. In this section, we compare the performance of the RWB and WB on simulated random elliptical images; the barycenters are computed via the IBP algorithm proposed in [10] and its free-support variant derived earlier in this paper. For any input image of $j \times \ell$ pixels, we can model it as a discrete probability measure supported on the grid $\{0, 1, \dots, j-1\} \times \{0, 1, \dots, \ell-1\}$. When computing the RWB and WB using the free-support variant of the IBP algorithm, we take the support of the barycenter to consist of R points in the space $[0, j-1] \times [0, \ell-1]$, where R denotes the number of support points we selected for the barycenter. Given the sparsity of the support of the barycenter, it is reasonable to select R that is smaller than the total number of grid points.

In the experiments, we generate $n = 200$ random nested ellipse images of size 40×40 pixels, each containing random perturbation points in the upper-right corner that serve as outliers. An example of such images is shown in Figure 1. To avoid potential information loss (which requires a sufficiently large number of barycenter support points) while keeping R from being excessively large, we tested various values of R and set $R = 105$. Furthermore, we also test various values of λ to evaluate the corresponding results. We observe that values of λ that are neither too large nor too small—i.e., those striking a balance between information loss and robustness—yield optimal performance, consistent with the findings reported in [4]. Finally, we set $\lambda = 5$ for the cost function $c^\lambda(\cdot, \cdot)$.

Additionally, in this experiment, we observed that the barycenter images computed using the W_1 distance are visually sharper than those obtained with W_2 . Therefore, all results presented below are computed with the W_1 distance.

From the results shown in Figure 2, we draw the following conclusions:

- (i) The boundaries of the Wasserstein barycenter near the random perturbation points become blurred, accompanied by a noticeable shift toward the disturbance.
- (ii) Under both free-support and fixed-support settings, the RWB exhibits sharper boundaries than the WB, with no obvious deviation toward the perturbation

points.

This numerical exercise confirms that the RWB is more robust to random perturbation points when computed on random ellipse images.

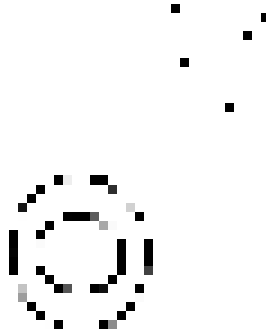


Figure 1: A random nested ellipse image with random outlier points in the upper-right corner.

5.2 Comparison of numerical data

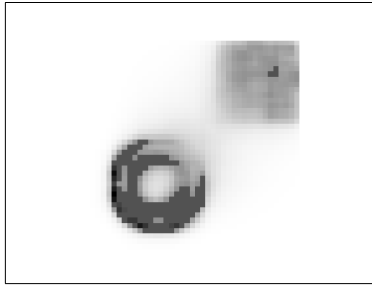
In the section, we demonstrate the variations of the RWB and the WB under different data contamination ratios through numerical simulations. In our experiment, we consider two source distributions: the first as the signal (Type 1 distributions) and the second as the contamination (Type 2 distributions):

$$\text{Type 1 : } N(\mu_0, \sigma_0), \mu_0 \sim U(-20, 20), \sigma_0 = 1$$

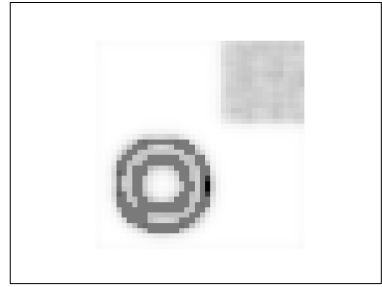
$$\text{Type 2 : } N(\mu_1, \sigma_1), \mu_1 \sim U(30, 70), \sigma_1 = 1$$

In this setting, the true Wasserstein barycenter of the signal is $\mathcal{N}(0, 1)$.

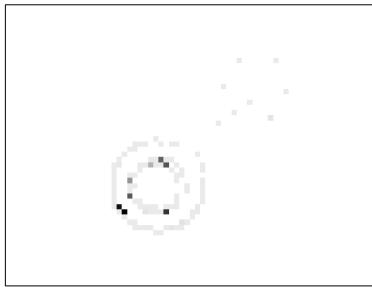
We begin by generating data from the signal and contamination distributions, resulting in a 100×1000 array, that is, 100 datasets, with each containing 1000 observations. Then we employ k -means clustering to generate support points. After empirical tuning over different values, we fix the number of support points to 100, and derive 100 input distributions by calculating the frequency of each dataset with respect to these support points. Finally, we only apply the original IBP algorithm to compute



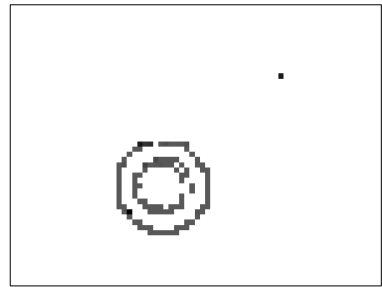
(a) Fixed-support WB



(b) Fixed-support RWB



(c) Free-support WB



(d) Free-support RWB

Figure 2: Barycenters of random nested ellipse images.

barycenters given the simplicity of this setting and the small number of support points. In addition, the cost function $c(\cdot, \cdot)$ is taken as the Euclidean distance, and we test various truncation values $\lambda \in \{10, 20, 30, 40, 50, 60, 70\}$ for the modified cost function $c^{(\lambda)}$, where 71.8 approximates the maximum value of the original cost matrix in this experiment. By analyzing the results under different values of λ shown in Figure 3 and Table 1, we observe that the RWB converges to the WB as λ increases, and the RWB achieves optimal performance at $\lambda = 30$ (since it yields the smallest value of mean Wasserstein distance (under different contamination ratios) between the RWB and true WB).

Figure 4 illustrates the variations in Wasserstein distance from both the WB and the RWB to the true Wasserstein barycenter and across data contamination ratios ranging from 0% to 25% in 1% increments. From the results shown in Figure 4, we draw the

following conclusions:

- (i) The Wasserstein distance from both the WB and RWB to the true-WB exhibit a monotonic increase with the growth of the data contamination test various ratio.
- (ii) The magnitude of variation in the WB curve is marginally larger than that in the RWB curve.

λ	10	20	30	40	50	60	70
W.distance.mean	1.0712	0.9448	0.9059	0.9748	1.0211	1.0598	1.0885

Table 1: Mean Wasserstein distance (under different contamination ratios) between the RWB and true WB across different values of λ .

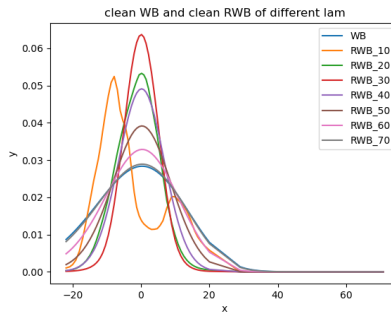


Figure 3: Distribution curves of WB and RWB.

In addition to the contamination case, the RWB also exhibits greater robustness than the WB in heavy-tailed cases. We thus examine data generated from the t-distribution $t(df, m, s)$, where df , m and s denote the degrees of freedom, location and scale, respectively. In this experiment, to ensure the existence of the second-order moment of the t-distribution (required in the \mathcal{W}_2 space), we set $df = 3$, $s = 1$, and $m \sim U(-50, 50)$. Similar to the contamination case, we test the truncation value λ within the range $\lambda \in \{30, 40, 50, 60, 70, 80, 90, 100, 110\}$. Among these values, $\lambda = 50$ yields the optimal result, as illustrated in Figure 5 and Figure 6. The

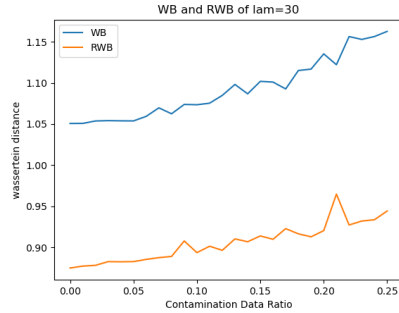


Figure 4: Wasserstein distance between WB (and RWB) and the true WB.

experiment demonstrates better performance of the RWB than the WB for heavy-tailed distributions.

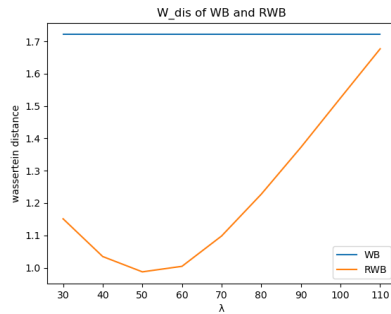


Figure 5: Wasserstein distance between WB (and RWB) and the true WB in heavy-tailed case.

In summary, the simulation results presented above indicate that the RWB outperforms the WB in terms of robustness under both contamination and heavy-tailed cases.

5.2.1 Real data analysis

In this section, we analyze the closing prices of the stock dataset in [27] and demonstrate the robustness of the RWB. We calculate the daily log-returns $r_t =$

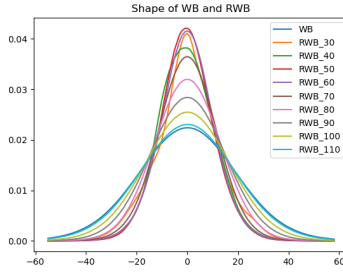


Figure 6: Distribution curves of WB and RWB in heavy-tailed case.

$\log(X_t/X_{t-1})$ for the closing prices X_t of each stock, and we obtain the distribution of r_t for each stock via kernel density estimation (KDE).

In practice, the values of r_t typically cluster around 0, yet this stock dataset contains several excessively large r_t values, which are clearly abnormal. Therefore, we use the Isolation Forest method proposed in [25] to identify critical thresholds for outliers, partitioning r_t into two subsets: *clean* and *out*. These two subsets are then combined to form the complete set of total r_t . Furthermore, we apply k-means clustering to select 190 points from the *clean* subset and 10 points from the *out* subset as support points, which are used to characterize the distribution of r_t for each stock. The total support set, denoted as $\text{support}_{\text{total}}$, is the union of $\text{support}_{\text{clean}}$ and $\text{support}_{\text{out}}$, comprising 200 support points in total. We then calculate the frequency distribution of the KDE for each stock over the $\text{support}_{\text{clean}}$ points, which serves as the input distribution under the clean case. Similarly, we compute the frequency distribution of the KDE for each stock over $\text{support}_{\text{total}}$, which is used as the input distribution under the outlier case.

For this setting, the barycenters derived from these input distributions enable us to observe the overall return distribution of stock closing prices corresponding to the market represented by the dataset.

Additionally, we compare the barycenters calculated from the outlier-included case with those from the outlier-free (*clean*) case to evaluate their robustness. Intuitively, a smaller deviation between the two scenarios indicates that the barycenter is less

influenced by outliers, implying stronger robustness.

As illustrated in Figure 7, the Wasserstein distance between $\text{RWB}_{\text{total}}$ and WB_{clean} remains consistently smaller than that between WB_{total} and WB_{clean} across various values of λ , exhibiting minimal variation. Furthermore, Figure 8 reveals that the shape of $\text{RWB}_{\text{total}}$ most closely approximates that of WB_{clean} when $\lambda = 0.30$. Consequently, we select $\lambda = 0.30$ as the optimal parameter, and the final barycenter results in Figure 9 demonstrate that $\text{RWB}_{\text{total}}$ aligns significantly closer to WB_{clean} than WB_{total} does. In summary, for this dataset containing substantial outliers, RWB proves to be significantly less susceptible to outliers than WB , thereby exhibiting superior robustness.

λ	0.28	0.30	0.32	0.34	0.36	0.38	0.40	0.42	0.44	0.46	0.48
W.distance	0.0641	0.0652	0.0661	0.0671	0.0679	0.0686	0.0694	0.0700	0.0706	0.0712	0.0717

Table 2: Wasserstein distance between RWB and the WB_{clean} across different λ .

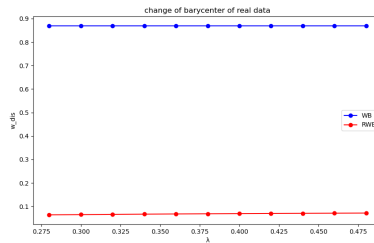


Figure 7: Wasserstein distance between the WB_{total} (and $\text{RWB}_{\text{total}}$) and the WB_{clean} across different λ .

6 Conclusions

This paper introduces the robust Wasserstein barycenter to mitigate the instability of the classical Wasserstein barycenter in the presence of outliers. We provide theoretical guarantees for the RWB , including its existence and consistency, and propose an effective computational method. Extensive numerical analysis, comprising both

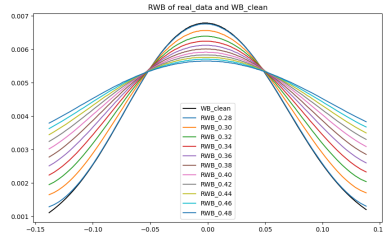


Figure 8: WB_{clean} and RWB_{total} across different λ .

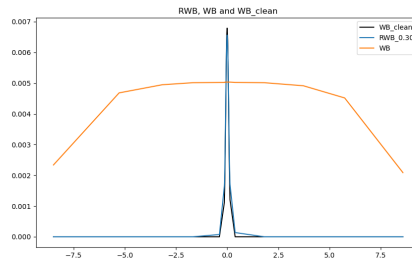


Figure 9: The figure illustrates the WB in the clean case, the WB_{total} and the RWB_{total} , where the RWB corresponds to $\lambda = 0.30$.

simulated and real-world data, illustrates that the RWB are significantly more robust than the standard WB, making it a compelling alternative for practical use. For future research, one may consider an entropy-regularized version of the RWB, and explore its theoretical and empirical performance in the presence of outliers and high dimensionality. Also, one may combine the RWB with current cutting-edge deep learning models.

References

- [1] Monge G. Mémoire sur la théorie des déblais et des remblais. *Mem. Math. Phys. Acad. Royale Sci.*, 1781: 666–704

- [2] Kantorovich L. On the Translocation of Masses. *Journal of Mathematical Sciences*, 2006, 133: 1381–1382
- [3] Fréchet M R. Les éléments aléatoires de nature quelconque dans un espace distancié. 1948
- [4] Ma Y M, Liu H, La Vecchia D. Inference via robust optimal transportation: theory and methods. *International Statistical Review*, 2025. Wiley Online Library
- [5] Billingsley P. *Convergence of Probability Measures*. Wiley, 1999
- [6] Arjovsky M, Chintala S, Bottou L. Wasserstein generative adversarial networks. In: *International Conference on Machine Learning*, 2017: 214–223. PMLR
- [7] Srivastava S, Li C, Dunson D B. Scalable Bayes via Barycenter in Wasserstein Space. *J. Mach. Learn. Res.*, 2015, 19: 8:1–8:35
- [8] Ramdas A, García Trillos N, Cuturi M. On Wasserstein Two-Sample Testing and Related Families of Nonparametric Tests. *Entropy*, 2017, 19: 47. MDPI
- [9] Altschuler J M, Boix-Adser E. Wasserstein barycenters are NP-hard to compute. *SIAM Journal on Mathematics of Data Science*, 2021, 4(1): 179–203
- [10] Benamou J-D, Carlier G, Cuturi M, et al. Iterative Bregman Projections for Regularized Transportation Problems. *SIAM Journal on Scientific Computing*, 2015, 37(2): A1111–A1138
- [11] Le Gouic J M. Existence and consistency of Wasserstein barycenters. *Probability Theory and Related Fields*, 2017, 168(3-4)
- [12] Agueh M, Carlier G. Barycenters in the Wasserstein Space. *SIAM Journal on Mathematical Analysis*, 2011, 43: 904–924
- [13] Mukherjee D, Guha A, Solomon J, et al. Outlier-Robust Optimal Transport. In: *International Conference on Machine Learning*, 2021: 7850–7860. PMLR
- [14] You K, Shung D, Giuffré M. On the Wasserstein Median of Probability Measures. *Journal of Computational and Graphical Statistics*, 2025, 34(1): 253–266
- [15] Cuturi M, Doucet A. Fast Computation of Wasserstein Barycenters. In: *Proceedings of the 31st International Conference on Machine Learning*, 2014, 32(2): 685–693. PMLR

- [16] Panaretos V M, Zemel Y. *An Invitation to Statistics in Wasserstein Space*. Springer, 2020
- [17] Kullback S, Leibler R A. On Information and Sufficiency. *The Annals of Mathematical Statistics*, 1951, 22(1): 79–86
- [18] Lin J. Divergence measures based on the Shannon entropy. *IEEE Transactions on Information Theory*, 1991, 37(1): 145–151
- [19] Vayer T, Gribonval R. Controlling Wasserstein Distances by Kernel Norms with Application to Compressive Statistical Learning. *Journal of Machine Learning Research*, 2023, 24(149): 1–51
- [20] Lindheim J V. Simple approximative algorithms for free-support Wasserstein barycenters. *Computational Optimization & Applications*, 2023, 85(1)
- [21] Carlier G, Ekeland I. Matching for teams. *Economic Theory*, 2010, 42: 397–418
- [22] Friesecke G, Penka M. The GenCol algorithm for high-dimensional optimal transport: general formulation and application to barycenters and Wasserstein splines. *SIAM Journal on Mathematics of Data Science*, 2023, 5(4): 899–919
- [23] Villani C. *Optimal transport: old and new*. Springer, 2009, 338
- [24] Prokhorov Y V. Convergence of Random Processes and Limit Theorems in Probability Theory. *Theory of Probability & Its Applications*, 1956, 1(2): 157–214
- [25] Liu F T, Ting K M, Zhou Z-H. Isolation forest. In: *2008 Eighth IEEE International Conference on Data Mining*, 2008: 413–422
- [26] Chewi S, Niles-Weed J, Rigollet P. *Statistical Optimal Transport: École d'Été de Probabilités de Saint-Flour XLIX – 2019*. Springer, 2025
- [27] Deamoner. Ultimate stock prediction machine learning training dataset. 2023. <https://github.com/Deamoner/ultimate-stock-machine-learning-training-dataset>